# Thermosphere densities derived from Swarm GPS observations

van den IJssel, Jose; Doornbos, Eelco; Iorfida, Elisabetta; March, Günther; Siemes, Christian; Montenbruck, Oliver

**DOI**
10.1016/j.asr.2020.01.004

**Publication date**
2020

**Document Version**
Accepted author manuscript

**Published in**
Advances in Space Research

**Citation (APA)**
van den IJssel, J., Doornbos, E., Iorfida, E., March, G., Siemes, C., & Montenbruck, O. (2020). Thermosphere densities derived from Swarm GPS observations. *Advances in Space Research*, *65*(7), 1758-1771. https://doi.org/10.1016/j.asr.2020.01.004

Journal Pre-proofs

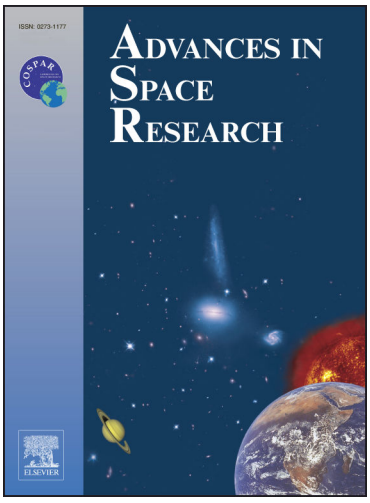


# Thermosphere densities derived from Swarm GPS observations

Jose den IJssel van, Eelco Doornbos, Elisabetta Iorfida, Günther March, Christian Siemes, Oliver Montenbruck

PII: S0273-1177(20)30007-7
DOI: https://doi.org/10.1016/j.asr.2020.01.004
Reference: JASR 14601

To appear in: *Advances in Space Research*

Received Date: 29 August 2019
Revised Date: 5 January 2020
Accepted Date: 8 January 2020

Please cite this article as: den IJssel, J. van, Doornbos, E., Iorfida, E., March, G., Siemes, C., Montenbruck, O., Thermosphere densities derived from Swarm GPS observations, *Advances in Space Research* (2020), doi: https://doi.org/10.1016/j.asr.2020.01.004

# Thermosphere densities derived from Swarm GPS observations

Jose van den IJssel[a,*], Eelco Doornbos[b], Elisabetta Iorfida[a], Günther March[a], Christian Siemes[a], Oliver Montenbruck[c]

[a] *Faculty of Aerospace Engineering, Delft University of Technology, Delft, The Netherlands*
[b] *Royal Netherlands Meteorological Institute (KNMI), De Bilt, The Netherlands*
[c] *Deutsches Zentrum für Luft- und Raumfahrt, Oberpfaffenhofen, Germany*

**Abstract**

After the detection of many anomalies in the Swarm accelerometer data, an alternative method has been developed to determine thermospheric densities for the three-satellite mission. Using a precise orbit determination approach, non-gravitational and aerodynamic-only accelerations are estimated from the high-quality Swarm GPS data. The GPS-derived non-gravitational accelerations serve as a baseline for the correction of the Swarm-C along-track accelerometer data. The aerodynamic accelerations are converted directly into thermospheric densities for all Swarm satellites, albeit at a much lower temporal resolution than the accelerometers would have been able to deliver. The resulting density and acceleration data sets are part of the European Space Agency Level 2 Swarm products.

To improve the Swarm densities, two modifications have recently been added to our original processing scheme. They consist of a more refined handling of radiation pressure accelerations and the use of a high-fidelity satellite geometry and improved aerodynamic model. These modifications lead to a better agreement between estimated Swarm densities and NRLMSISE-00 model densities. The GPS-derived Swarm densities show variations due to solar and geomagnetic activity, as well as seasonal, latitudinal and diurnal variations. For low solar activity, however, the aerodynamic signal experienced by the Swarm satellites is very small, and therefore it is more difficult to

*Corresponding author
*Email address:* j.a.a.vandenijssel@tudelft.nl (Jose van den IJssel)

accurately resolve latitudinal density variability using GPS data, especially for the higher-flying Swarm-B satellite. Therefore, mean orbit densities are also included in the Swarm density product.

*Keywords:* Swarm; GPS; thermosphere density

## 1. Introduction

The European Space Agency (ESA) Swarm mission was launched on 22 November 2013 to measure the dynamics of the Earth's magnetic field and its interaction with the Earth system (Friis-Christensen et al., 2008). A secondary mission objective of Swarm is to derive information about the thermospheric density and winds (Visser et al., 2013). With three identical satellites flying in near-polar low Earth orbits, the Swarm mission can deliver very useful information about the thermosphere. The top part of figure 1 shows the evolution of the orbit altitude of the Swarm satellites over time. Swarm-B flies at a relatively high altitude of about 510 km, while the other two satellites fly side-by-side at a lower initial altitude of 480 km, and are therefore more affected by atmospheric drag. The bottom part of figure 1 shows that the orientation of the orbit planes of the upper satellite and lower pair were equal at the start of the mission, but have slowly drifted apart over time, which significantly increases the coverage of local solar times. This extensive coverage of altitudes and local times will be of benefit for the improvement of thermosphere density models when Swarm density data are assimilated.

To obtain thermospheric density and wind information, the scientific payload of the Swarm satellites includes electrostatic accelerometers (Fedosov and Peřestý, 2011). Located at the center of mass of the satellite, such instruments are able to measure very precisely the non-gravitational accelerations acting on the satellite. These measurements can be used for thermospheric density retrieval, as has been shown by the earlier CHAMP, GRACE and GOCE missions (Bruinsma et al., 2004; Sutton et al., 2007; Doornbos et al., 2010; March et al., 2019a). Unfortunately, the Swarm accelerometers are suffering from many issues that affect the quality of their observations. Siemes et al. (2016) have shown that the Swarm accelerometers are perturbed by a number of anomalies, including spikes, sudden changes in the accelerometer bias, and large temperature-induced bias variations. This significantly affects their usefulness for density retrieval.

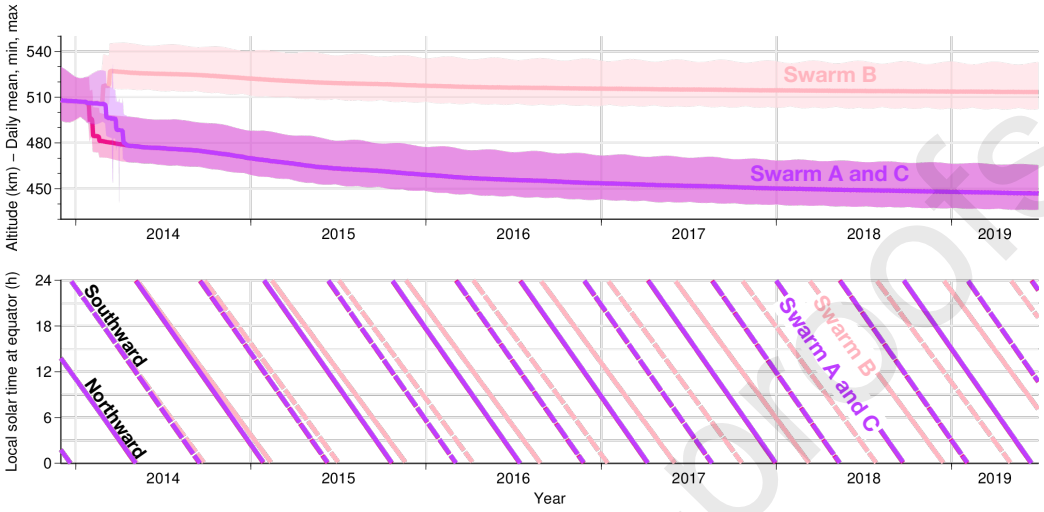


Figure 1: Evolution of the Swarm satellite orbits, with daily average altitude above the GRS80 reference ellipsoid (top), and local time at equator crossings (bottom).

In addition to accelerometers, all Swarm satellites are equipped with high-quality Global Positioning System (GPS) receivers, which are developed by RUAG Space (Zangerl et al., 2014). These receivers have eight channels available for dual-frequency tracking and operate with almost continuous data availability. Initially, the Swarm GPS data rate was set to 0.1 Hz, but on 15 July 2014 this has been increased to 1 Hz. Several other modifications have also been uploaded to the on board GPS receivers, to further increase their performance. These consist of changes in the GPS antenna Field of View (FoV), in order to increase the tracking performance, as well as several tracking loop modifications, in order to improve the robustness of the receiver to ionospheric scintillation (Van den IJssel et al., 2016).

The Swarm GPS observations are used for precise positioning and time tagging of the magnetic and electric field instrument measurements, as well as for the determination of the Earth's gravity field and the slant total electron content (Van den IJssel et al., 2015; Teixeira da Encarnação et al., 2016). In addition, because of the many anomalies in the accelerometer data, an alternative approach has been developed, where the non-gravitational accelerations experienced by the satellites are derived from the high-quality

GPS data, instead of directly measured by the accelerometers. These estimated accelerations are used to correct and augment the accelerometer observations, which are currently available for Swarm-C only. These merged GPS-accelerometer accelerations are used to generate high resolution thermospheric densities for this satellite (Siemes et al., 2016). In addition, the GPS-derived accelerations are used to generate GPS-only thermospheric densities. These densities do not have the high temporal resolution that can be obtained with an accelerometer, but they are available for all three satellites.

In recent years, several authors have shown that thermospheric density data can be derived from precise GPS tracking data of satellites in low Earth orbit. Kuang et al. (2014) use a GPS-based precise orbit determination to estimate accelerations due to drag. These accelerations consist of a long-period correction to a nominal drag model as well as short-period corrections from estimated residual accelerations with a 5 minute update time. The resulting drag accelerations are converted to densities using a constant drag coefficient that is obtained from a best fit with a nominal drag model. They have applied their method to data from several satellites and demonstrate that it can provide useful neutral density measurements for satellite altitudes up to 715 km, with a precision and resolution that is lower than obtained from on board accelerometers.

McLaughlin et al. (2013) use a method that eliminates the more complex handling of GPS data observations. Instead they use precise satellite orbits as pseudo-observations in an orbit determination scheme to estimate corrections to a baseline density model. Using a sequential filtering scheme, corrections to both the density and the ballistic coefficient are estimated simultaneously. They show that the estimated density is sensitive to the selected nominal ballistic coefficient, and this might lead to a bias in the estimated density. Calabia and Jin (2017) do not make use of an orbit determination approach, instead they derive non-gravitational accelerations from the numerical differentiation of reduced-dynamic precise orbit velocities. They have validated their approach with GRACE accelerometer data and show that their orbit-derived densities are within 10% compared to the more accurate accelerometer-derived densities.

This paper presents an alternative method to derive density data from GPS tracking data, which is applied to data from the Swarm satellites. Section 2 describes the strategy that is used to estimate thermospheric densities from the Swarm GPS observations. Two modifications in this strategy which have been implemented recently will be explained in detail. They consist of

a more refined handling of the solar and Earth radiation pressure modelling, which is especially important for the current solar minimum conditions, as well as an improved modelling of the satellite geometry and the gas-surface interactions. In section 3, the resulting GPS-derived densities for the entire mission are presented and the impact of the recent modifications on their accuracy is assessed. Finally, the paper concludes with a short summary of the results and gives recommendations for further improvements.

## 2. Processing strategy

The processing strategy that is implemented to derive thermospheric densities from the Swarm GPS observations consists of two steps. In the first step, explained in section 2.1, non-gravitational accelerations are estimated in a GPS-based precise orbit determination. In the second step, explained in section 2.2, these accelerations are converted into thermospheric densities.

### *2.1. Non-gravitational acceleration retrieval from GPS data*

This section describes the Precise Orbit Determination (POD) strategy that is used to convert the range and phase information in the Swarm GPS measurements into non-gravitational accelerations. This strategy is based on an extended Kalman filter approach, which is implemented in the GPS High-precision Orbit determination Software Tools (GHOST) developed by the Deutsches Zentrum für Luft- und Raumfahrt (DLR) (Wermuth et al., 2010). The applied Kalman filter implementation makes use of a forward and backward run, and a final smoother run delivers the optimal combination of these two runs (Montenbruck et al., 2005). This approach has already been successfully used for the estimation of non-gravitational accelerations from the GPS data of the GOCE satellite during its reentry phase (Visser and Van den IJssel, 2016).

Table 1 lists the details of the processing standards used for the estimation of non-gravitational accelerations. An undifferenced POD approach is used, in which the GPS orbits and clocks are kept fixed to the final values computed by the Center for Orbit Determination in Europa (CODE) (Dach et al., 2009, 2018). To eliminate the first-order ionospheric effect, the ionosphere-free linear combination of GPS code and carrier phase measurements at two frequencies is used. For the GPS transmitter satellites, absolute antenna phase offsets and corrections are taken into account according to the International GNSS Service (IGS) standards (Schmid et al., 2016), while for the

Swarm satellites, an inflight calibration map has been applied (Van den IJssel et al., 2016). The attitude of the Swarm satellites is constructed from the on board star tracker observations.

The gravitational force models include GOCO03s for the global Earth gravity field (Mayer-Gürr et al., 2012), FES2004 for ocean tides (Lyard et al., 2006), IERS2003 conventions for solid Earth and pole tides (McCarthy and Petit, 2004) and $3^{rd}$ body perturbations by the Sun and Moon. In the nominal approach, no force models are included for non-gravitational accelerations. Instead, smooth empirical accelerations with an update interval equal to the GPS data rate (0.1 or 1 Hz) are used to capture the total non-gravitational signal. These accelerations are modeled as Gauss-Markov processes defined by a steady-state variance $\sigma_a$, process noise $\sigma_p$ and correlation time $\tau$. The tuning of these parameters was obtained by a careful trial-and-error process based on several quality indicators, such as consistency in orbit overlaps in terms of estimated accelerations and position solution, as well as consistency with the Swarm precise science orbits and satellite laser ranging observations.

In along-track direction, where the satellites encounter the largest non-gravitational signal, relatively large values are used for these parameter values ($\sigma_a = 300$ nm/s$^2$, $\sigma_p = 10$ nm/s$^2$, $\tau = 5610$ s). Although the orbital position is most sensitive to perturbing accelerations in the along-track direction, a long correlation time of about one orbit is selected for these accelerations, because it was noticed that for short correlation times, the estimated accelerations do not show a proper amplitude. This was also visible in the GRACE results presented in Montenbruck et al. (2005). In the other orbit directions, smaller values are used (radial: $\sigma_a = 10$ nm/s$^2$, $\sigma_p = 5$ nm/s$^2$, $\tau = 360$ s, cross-track: $\sigma_a = 10$ nm/s$^2$, $\sigma_p = 5$ nm/s$^2$, $\tau = 60$ s). In addition to these empirical accelerations, the estimated parameters also include the initial state, epoch-wise GPS receiver clock offsets and carrier-phase float ambiguities per observation tracking pass. To avoid a possible degraded orbit quality at the edges of the orbit arc, the orbits are computed using 30 h batches, with 6 h overlaps between consecutive orbits. Only the center daily 24 h part of the arc is used for density retrieval.

To obtain the aerodynamic accelerations which are used to determine thermospheric densities, the accelerations due to solar and Earth radiation pressure have to be subtracted from the estimated total non-gravitational accelerations. In the nominal approach, these radiation pressure accelerations have been computed and subtracted in post-processing, using force models, which have been evaluated along the Swarm orbits. An overview of these mod-

Table 1: Processing standards for total non-gravitational acceleration retrieval in black. For the retrieval of aerodynamic accelerations the standards indicated in blue are also included.

| Model | Description |
|---|---|
| **GPS measurement model** | |
| GPS tracking data | undifferenced ionosphere-free code & phase observations |
| GPS ephemeris | CODE final GPS orbits & 5 s clocks |
| GPS antenna phase model | igs08.atx (up to Jan 2017) & igs14.atx |
| Receiver antenna phase model | inflight calibration map |
| **Gravitational forces** | |
| Earth gravity | GOCO03s (150x150) |
| Solar Earth & Pole tides | IERS2003 conventions |
| Ocean tides | FES2004 (30x30) |
| Luni-solar gravity | analytical ephemerides |
| **Non-gravitational forces** | |
| Solar radiation | conical Earth shadow model |
| Earth radiation | CERES Earth radiation model |
| **Satellite model** | |
| Mass | satellite mass history data |
| Surface model | 15-panel macro model |
| **Reference frame** | |
| Earth orientation | CODE final ERP |
| Satellite attitude | star tracker data |
| **Estimation** | |
| Methodology | extended Kalman filter |
| Arc length | 30 hours |
| Estimated parameters | initial state & epoch-wise clock offsets<br>float carrier phase ambiguities<br>3D empirical accelerations |

els is also listed in table 1. For solar radiation pressure, a conical shadow model with umbra/penumbra transitions is used, while an approach according to Knocke et al. (1988) is used to model the Earth radiation pressure. A polynomial approximation of the Clouds and Earth's Radiant Energy System (CERES) data is used to determine the Earth's emmissivity and reflectivity. The Swarm satellite surface is modelled by a 15-panel macro model, with for each panel accompanying properties for absorbed, diffusely reflected, and specularly reflected photons in the visual and infrared regime based on data from the satellite manufacturer (Siemes, 2019). For surfaces covered with multi-layer insulation, which includes all panels except for the solar arrays, spontaneous re-emission of absorbed radiation is taken into account according to Cerri et al. (2010). A similar modelling of solar and Earth radiation pressure for the Swarm satellites was also applied in Montenbruck et al. (2018).

The estimated non-gravitational accelerations from the Kalman filter approach are relatively smooth, while the modelled radiation pressure accelerations can contain sharp jumps at e.g. eclipse transitions. In order to not introduce artifacts, a smoothing also needs to be applied to the modelled radiation pressure accelerations, before they are subtracted in post-processing. The incompatibility of this smoothing introduces an error, which is negligible when the aerodynamic signal is very large. Figure 2 shows that this is indeed the case in the early phase of the Swarm mission. However, for the current solar minimum conditions, both aerodynamic and radiation pressure accelerations are of similar magnitude, especially for the higher-flying Swarm-B satellite. In this case, it is very important to reduce all possible error sources in the modelling of the radiation pressure accelerations.

Therefore, in addition to our original processing chain, a second POD processing chain was recently implemented, in which aerodynamic accelerations are estimated directly from the GPS observations. In this chain, the accurate modelling of the solar and Earth radiation pressure accelerations is included in the POD and empirical accelerations estimate the remaining aerodynamic-only accelerations. This approach has the benefit that the radiation pressure models are included at full resolution, and removes errors due to incompatibilities in smoothing. It is expected that this will also benefit the assessment of future improvements to the Swarm radiation pressure modelling, as errors in the radiation pressure satellite model geometry and optical properties are no longer convoluted with smoothing errors. Note that the original processing chain for the retrieval of total non-gravitational

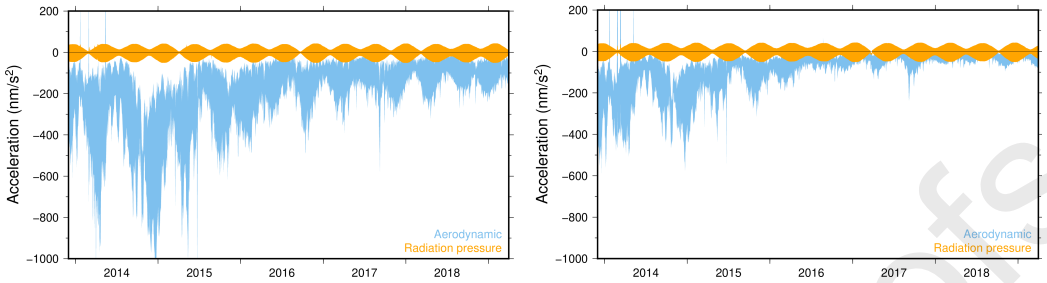


Figure 2: Time series of modelled aerodynamic and solar radiation pressure accelerations for Swarm-C (left) and Swarm-B (right).

accelerations is maintained, as they are necessary to correct and augment the accelerometer observations. A different approach to derive total non-gravitational accelerations experienced by satellites is presented in Bezděk et al. (2018) and Vielberg et al. (2018). Their approach is based on the numerical differentiation of kinematic orbits and uses the Savitzky-Golay filter to reduce the impact of noise. However, these accelerations have only been used to calibrate the accelerometer observations of the GRACE and Swarm missions, and have not been used to derive thermospheric densities directly.

To assess the performance of the radiation pressure models, a dynamic POD test was performed where these models are included, together with a state-of-the art aerodynamic model. For this test, the NRLMSISE-00 atmospheric density model was selected (Picone et al., 2002), and Sentman's formulation was used for the computation of the drag and lift forces over all panels of the satellite macro model (Sentman, 1961a,b). Instead of empirical accelerations, a global scale factor was estimated for both the solar radiation modelling ($f_R$) and aerodynamic modelling ($f_D$). No reliable scale factor can be estimated for the Earth radiation modelling (Montenbruck et al., 2018), therefore this factor was kept fixed to one. In case the aerodynamic and radiation pressure forces are properly modelled, the estimated scale factors should be equal to one.

Figure 3 shows the estimated scale factor results for Swarm-B for a period of approximately 9 months in 2017-2018. This period was selected to cover all $\beta$ angles (i.e. the angle between the orbit plane and the Sun) and had relatively low solar activity, with a mean solar activity proxy $F_{10.7}$ value of 75 sfu (see also the bottom part of figure 7). This reduces the possibility that errors in the aerodynamic modelling affect the solar radiation pressure scale

factor estimation. The resulting $f_D$ of about $0.562 \pm 0.074$ indicates that the aerodynamic model significantly overestimates the satellite drag. The value of about $1.054 \pm 0.064$ for $f_R$ indicates that the solar radiation pressure is relatively well modelled. However, small variations in the estimated $f_R$ are visible, which are correlated with the $\beta$ angle. This indicates that further improvements in solar radiation pressure modelling are still possible.

A similar dynamic POD test has also been performed for Swarm-C. For this satellite, an estimated $f_D$ value of $0.538 \pm 0.072$ was found, together with a $f_R$ of $1.077 \pm 0.118$. As expected, the estimation results of these identical satellites are comparable, but the $f_R$ estimation of Swarm-C shows a larger standard deviation. This indicates that for the lower-flying satellite the $f_R$ estimation is indeed more affected by aerodynamic modelling errors. For the estimation of the aerodynamic accelerations in the second POD chain, a fixed scale factor of 1.05 has therefore been applied to the solar radiation pressure modelling of all three Swarm satellites. In this chain, the parameters of the empirical accelerations are also slightly adapted, to take the smaller aerodynamic signal compared to the total non-gravitational signal into account. In along-track direction the process noise is reduced from 10 to 8 $\mathrm{nm/s^2}$, while in radial direction it is reduced from 5 to 4 $\mathrm{nm/s^2}$.

### *2.2. Thermosphere density retrieval from acceleration data*

This section describes the conversion of non-gravitational accelerations to thermospheric densities. In case total non-gravitational accelerations are estimated, the accelerations due to radiation pressure first have to be removed, in order to get the aerodynamic accelerations. As mentioned in section 2.1, this is done using modelled radiation pressure accelerations along the Swarm orbit. These radiation pressure models are generally much more accurate than thermospheric density models, which can have uncertainties of 15 to 30%, depending on altitude and solar and geomagnetic activity levels (Marcos et al., 1994), but can be off by up to a factor of 2 during deep solar minimum, as demonstrated by the estimated scale factors in figure 3 and comparable results for CHAMP and GRACE in 2008 (Doornbos, 2012). For the relatively smooth GPS-derived accelerations, a smoothing is applied to the radiation pressure accelerations before they are subtracted in post-processing. This is not necessary for the merged GPS-accelerometer accelerations, due to the high-frequency information contained in the accelerometer observations.

To convert the aerodynamic accelerations into thermospheric densities, the direct approach as described by Doornbos et al. (2010) is used. With the

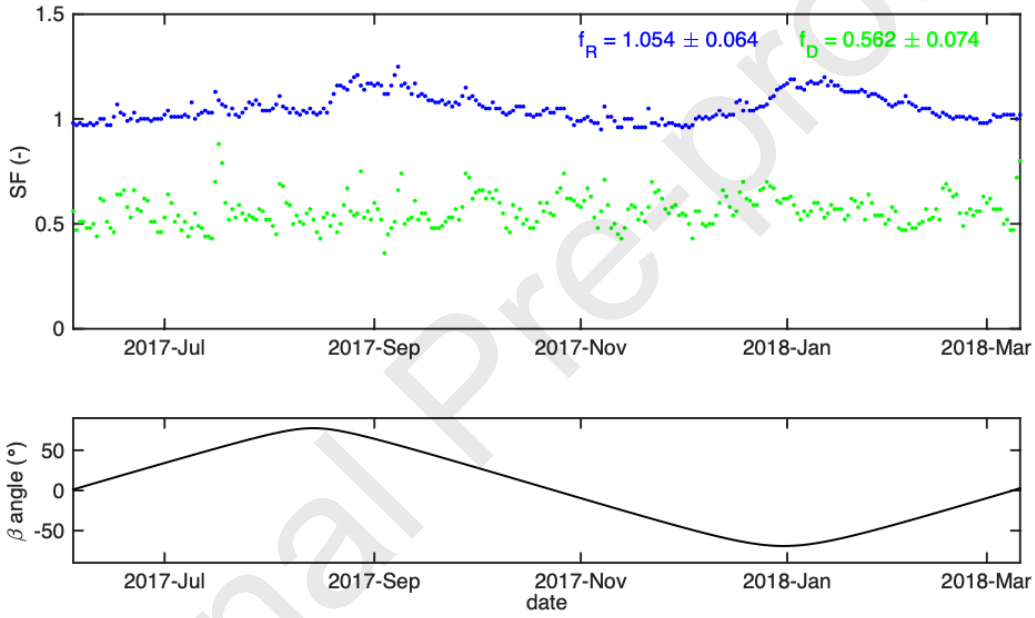


Figure 3: Estimated scale factors $f_R$ and $f_D$ results from a dynamic POD (top) and accompanying $\beta$-angles (bottom) for Swarm-B.

iterative approach, also described by Doornbos et al. (2010), it is possible to solve for crosswinds in addition to thermospheric densities. This approach has been successfully used to determine crosswinds for the CHAMP and GRACE satellites (Doornbos, 2012), as well as for the GOCE satellite (Visser et al., 2019). Unfortunately, for Swarm this iterative approach cannot be used, because accurate accelerometer data are not available in the directions perpendicular to the flight direction. In addition, it is expected that the GPS-derived accelerations in these directions are not accurate enough and do not have sufficient temporal resolution to recover the relatively small and fast-changing wind signal along the orbit.

With the direct approach, only the observed aerodynamic accelerations in flight direction are considered and compared with modelled aerodynamic accelerations along the Swarm orbit. The modelled aerodynamic accelerations can be computed as follows

$$\mathbf{a_{aero}} = \mathbf{C_a} \frac{A_{ref}}{m} \frac{1}{2} \rho v_r^2 \tag{1}$$

In this equation, $m$ refers to satellite mass, $A_{ref}$ is the reference area of the satellite, $\rho$ is the thermospheric density and $v_r$ is the relative velocity of the atmosphere with respect to the spacecraft, which is the sum of the contributions from the velocity of the satellite, the corotating atmosphere and winds. Accurate wind velocity observations are not available for Swarm, and therefore this information is obtained from the horizontal wind model HWM07 (Drob et al., 2008). The force coefficient vector $\mathbf{C_a}$ is a function of the satellite shape, its orientation with respect to the flow and the nature of the aerodynamic interaction with the atmospheric particles (Doornbos et al., 2010). Note that when lift and sideways forces are ignored, the aerodynamic acceleration reduces to the drag acceleration. In this case, the force coefficient vector $\mathbf{C_a}$ can be written as the scalar drag coefficient $C_D$.

In the original processing strategy, the computation of $\mathbf{C_a}$ was based on Sentman's formulation for the computation of lift and drag forces acting on the satellite outer surfaces, which are approximated by the 15-panel macro model (Sentman, 1961a,b). Knowledge about the relative concentration of the different particle species in the atmosphere, as well as the atmospheric temperature, is also required to determine $\mathbf{C_a}$. Unfortunately, in situ observations of these parameters are not available for Swarm, and therefore this information is taken from the NRLMSISE-00 model. For each observed aerodynamic acceleration, the thermospheric density of the modelled aero-

dynamic acceleration is then adjusted in order to match the modelled and observed accelerations, and in this way estimated densities are obtained.

The simplified macro model, however, cannot accurately describe the full satellite outer geometry, and this will limit the accuracy and consistency of the derived densities. The macro model is also not able to model multiple reflections and shadowing effects, and this introduces systematic errors at the level of 5-15% (Doornbos, 2012). Therefore, the computation of the force coefficient vector $\mathbf{C_a}$ has recently been updated to include a more realistic high-fidelity geometry and aerodynamic model, based on the Stochastic Parallel Rarefied-Gas Time-Accurate Analyzer (SPARTA) code for the analysis of rarefied aerodynamics (Gallis et al., 2014). Figure 4 shows the new 3D model that has been developed for the Swarm satellites based on technical drawings from the satellite manufacturing company and pre-launch pictures (March et al., 2019a). Compared to the 15-panel macro model, the new geometry model gives a more realistic representation of the Swarm satellite surface. This high-fidelity geometry model is used as input for the SPARTA gas-dynamics simulator, which is based on a Monte-Carlo approach. A comparison of the panel and the new SPARTA model by March et al. (2019a) shows that a scale difference of about 30% exists between the two, where the SPARTA model is considered to be more accurate. Note that a scale factor has meanwhile already been applied to the panel model densities in the nominal processing to account for this 30% difference.

Although March et al. (2019a) assumed full accommodation for the gas-surface interactions, for the processing of Swarm densities the value of the accommodation coefficient is set to 0.93. This value is also used in earlier work of Doornbos et al. (2010). The value of the accommodation coefficient depends on adsorbed gas composition over satellite surfaces, which in turn could depend on altitude and solar activity level (Pardini et al., 2010; Pilinski et al., 2010). According to Mehta et al. (2017) variations in drag and density up to 20% are possible due to changes in the accommodation coefficient for satellites such as GRACE. Because of a lack of direct measurement data, it is extremely difficult to implement a well-validated time-varying gas-surface interaction parameterisation. A fixed accommodation coefficient value of 0.93 has previously been adopted as a sort of de-facto standard, after use in a numerical example, thought suitable for solar maximum periods (Sutton, 2008; Bowman et al., 2007). This value is maintained in this work. However, analysis from March et al. (2019b), based on thermospheric wind retrieval from CHAMP and GOCE accelerometer data, indicates that the optimal

Figure 4: Rendering of the March et al. (2019a) high-fidelity 3D outer surface geometry model for Swarm.

value for the energy accommodation coefficient might be lower. A parallel analysis is currently performed to determine a reliable value for the whole Swarm mission, which will be taken into account in future data processing updates.

## 3. Results

With the processing strategy outlined in the previous section, GPS-derived densities are computed for all Swarm satellites, which are available as Level 2 product on the official ESA Swarm website (ftp://swarm-diss.eo-int). In addition, the estimated total non-gravitational and aerodynamic accelerations are also available as Level 2 product for all Swarm satellites. Both Level 2 products are delivered in daily 24 h files with a 30 s sampling. Note that the 30 s sampling of the accelerations is obtained by downsampling the original 0.1 or 1 Hz data rate of these estimated accelerations.

It has to be stressed that the 30 s sampling rate does not reflect the actual signal information that is available in the GPS-derived acceleration data. Figure 5 shows the power spectral density (PSD) of the estimated aerodynamic accelerations obtained with the original approach, in which total accelerations are estimated and smoothed radiation pressure accelerations are subtracted, as well as the new approach, where the aerodynamic accelerations are estimated directly. For comparison, figure 5 also shows modelled aerodynamic accelerations. These accelerations are obtained using the NRLMSISE-00 atmospheric density model together with the satellite surface macro model as described in section 2.1. It is clear that the higher-frequency signals that are present in the modelled accelerations are not well recovered

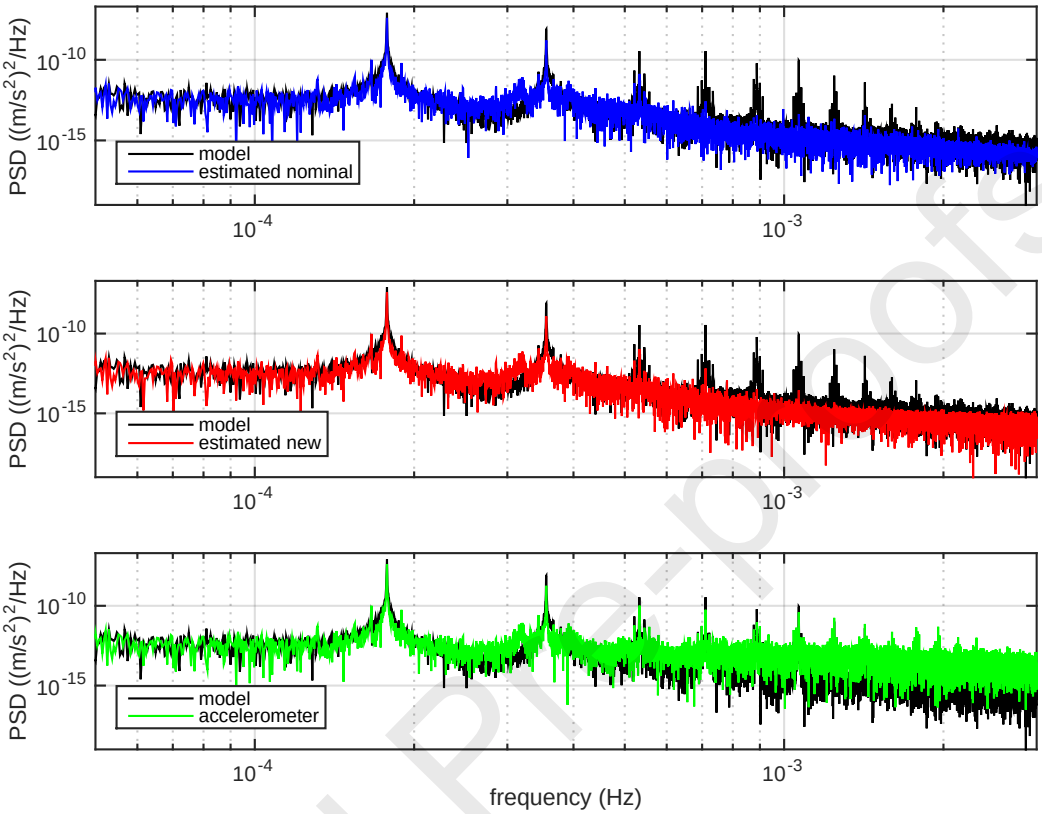


Figure 5: Power spectral density of Swarm-C aerodynamic accelerations for December 2014 using the original strategy (top), the direct estimation (middle), and derived from the merged GPS-accelerometer observations (bottom). The modelled aerodynamic accelerations are also shown as reference.

in the GPS-derived accelerations. Peaks of up to 4-5 cycles per revolution are visible in the PSD of the GPS-derived accelerations, which means that the temporal resolution of the recovered aerodynamic signal is about 20 minutes. As a reference, the bottom part of figure 5 also shows the PSD of the aerodynamic accelerations that are derived from the merged GPS-accelerometer data. For these accelerations, the low frequency signal is obtained from the GPS data, while the accelerometer data delivers the high frequency information (Siemes et al., 2016). In this case, also the higher harmonics of the orbital frequency are recovered.

Figure 6 shows the GPS-derived densities for Swarm-C since the start of the mission until the end of July 2019. These densities have been obtained

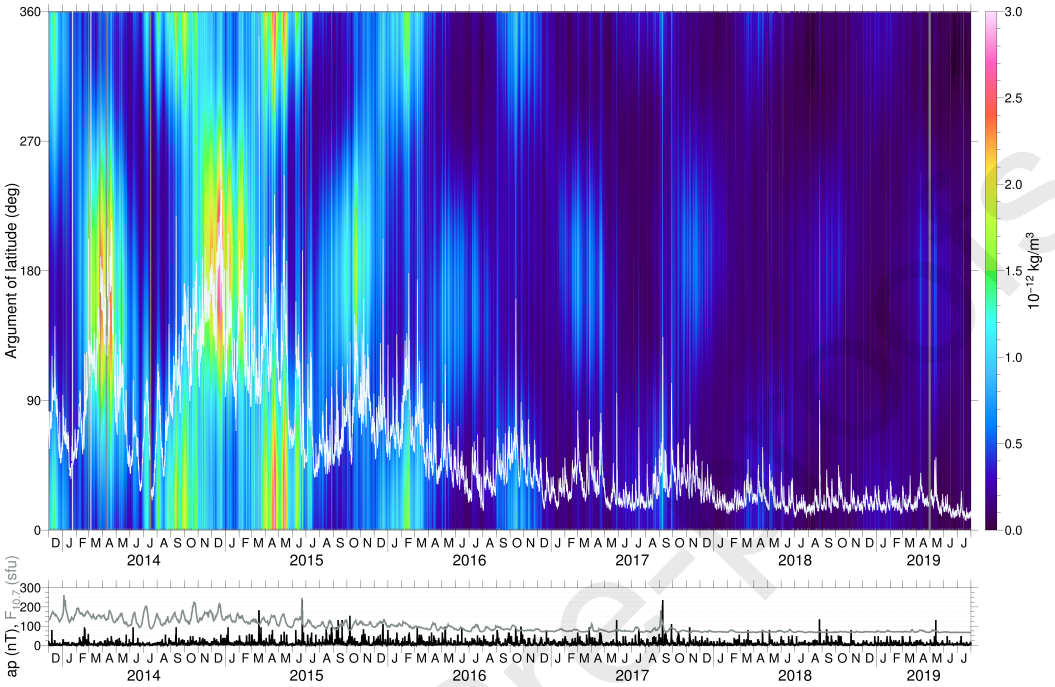


Figure 6: Time series of estimated density for Swarm-C (top), and solar activity proxy $F_{10.7}$ and geomagnetic index $ap$ (bottom). The white line indicates the mean orbit density, with values that refer to the scaling of the color bar.

with the latest processing strategy, which includes the direct estimation of aerodynamic accelerations in the POD and the use of the high-fidelity satellite geometry and aerodynamic model. Each vertical line in figure 6 represents a single orbital revolution, where the North and South Poles are crossed at 90° and 270° argument of latitude, respectively. As a reference, the bottom part of figure 6 shows the solar activity proxy $F_{10.7}$ and the geomagnetic index $ap$. Density variations due to solar and geomagnetic activity, as well as seasonal, latitudinal and diurnal variations can be recognized. Highest densities are obtained in the early mission phase, due to the relatively high solar activity in this period. Clear day-to-night variations in density are visible, with larger densities in the sunlit hemisphere compared to the dark hemisphere. During the current solar minimum conditions the Swarm-C satellite experiences very low densities. A few recent storms are, however, still clearly visible in the recovered densities.

As expected, the Swarm-B satellite, which is flying at a more than 50 km

higher altitude compared to Swarm-C, experiences lower densities, due to the exponential decrease of thermospheric density with altitude. This can be seen in figure 7, which shows the time series of GPS-derived densities for Swarm-B. Compared to figure 6 the scaling in this figure is adjusted by a factor of two, to take the significantly reduced density signal into account. For the current solar minimum conditions, the satellite experiences densities below $10^{-13}$ kg/m$^3$, which are visible in figure 7 as the deep purple and black areas. With such a small signal, it becomes challenging to derive accurate densities and small inaccuracies in the processing occasionally lead to unrealistic negative densities. Therefore, mean orbit densities are also computed, using a moving average of the estimated densities with a window length of one orbital period. In this way, a higher accuracy is obtained at the cost of a lower temporal resolution. These mean orbit densities are also depicted in figures 6 and 7 as white lines and show reliable results even for very low solar activity. The mean orbit densities are also included as additional field in the available Level 2 density product for all Swarm satellites.

Finally, figure 8 shows the impact of the two recent modifications that were implemented in the density processing strategy. This impact is assessed by a correlation analysis between the estimated and modelled densities for both Swarm-C and Swarm-B. In this analysis, the modelled densities are again obtained using the NRLMSISE-00 thermospheric density model. The top part of figure 8 shows the correlation between the modelled and estimated densities obtained using the original processing strategy, without the two recent processing modifications. In the middle part of figure 8, the correlation results are shown for the estimated densities which are obtained with the direct estimation of aerodynamic accelerations in the processing strategy. Finally, the bottom part of the figure shows the correlation results for the estimated densities obtained with the latest processing strategy, which also includes the new satellite geometry and aerodynamic model. For this correlation analysis, all data for 2018 have been used, which is a period with low solar activity. It is expected that for such a low solar activity period, the impact of the improved handling of radiation pressure accelerations will be more significant.

In each part of figure 8, on the horizontal axis the histogram of the estimated densities is shown in black, while the vertical axis shows the histogram of the modelled densities. For easy comparison, the histogram corresponding to the other data set is also shown in grey on both axes. The 3D histogram in color shows the correlation between the two density data sets. In addi-

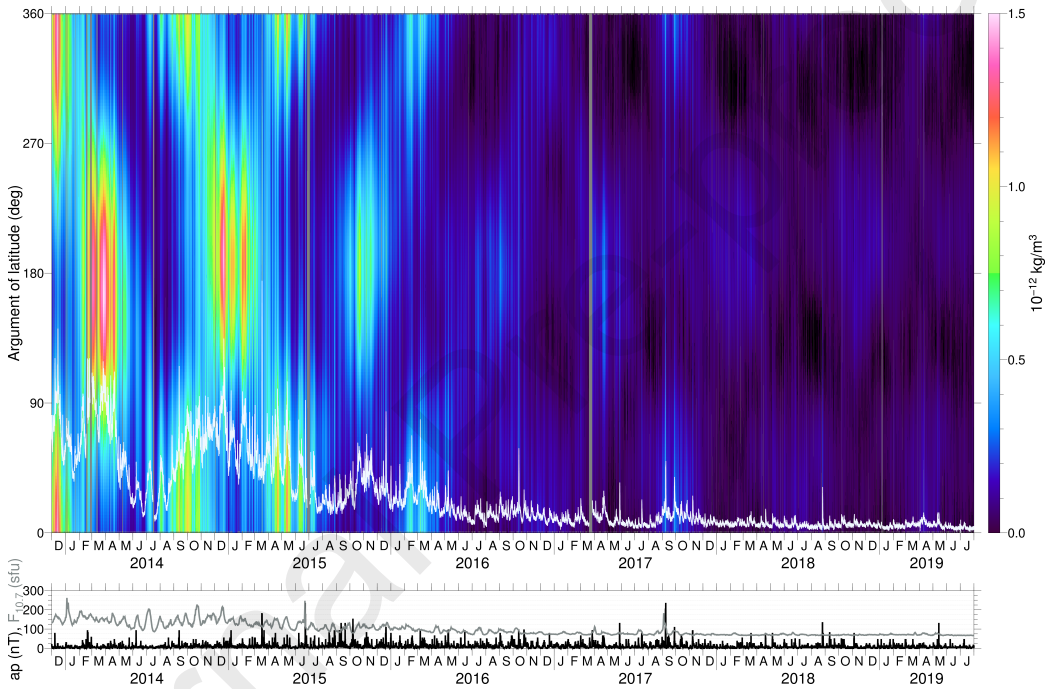


Figure 7: Time series of estimated density for Swarm-B (top), and solar activity proxy $F_{10.7}$ and geomagnetic index $ap$ (bottom). The white line indicates the mean orbit density, with values that refer to the scaling of the color bar.

tion, each figure presents the number of data points $n$, the correlation value $p$, as well as the log normal mean $\mu^*$ of the density ratios, which indicates the offset of the cloud of data points with respect to the central diagonal, and the log normal standard deviation $\sigma^*$ of the density ratios, which is a measure of the width of the cloud.

With the original processing strategy, the estimated densities of Swarm-C have a correlation of 0.64 with the model densities. For lower densities, the cloud of data points is more noisy, mainly due to the higher contribution of solar radiation pressure modelling errors compared to the aerodynamic signal. The mean of the density ratios is 0.53, which indicates that there is a significant scaling issue between the two sets of densities. This suggests that the NRLMSISE-00 model overestimates the density, which is in agreement with the results that were obtained in the dynamic POD test described in section 2.1, where a drag scale factor of about 0.56 was found using the same model. When the direct estimation of aerodynamic accelerations is included in the processing, the correlation between the estimated and modelled densities improves significantly to 0.76. The value of 0.56 for the mean of the density ratios is also closer to the value found for the dynamic POD test. Furthermore, the standard deviation of the density ratios reduces significantly from 1.70 to 1.48. Including the new satellite geometry and aerodynamic model in the conversion of aerodynamic accelerations to densities does not have a large impact on the correlation and standard deviation of the density ratios, while the mean of the density ratios is slightly larger. However, it has to be kept in mind that this modification was already to a large extent included in the original processing strategy by applying a scale factor.

For Swarm-B, the correlation between the estimated and modelled densities is worse compared to Swarm-C, which can be explained by the significantly reduced density signal for this higher-flying satellite. With the original processing strategy, the correlation between the two densities is only 0.45, and this improves to 0.50 when the latest processing strategy is used. Note that the number of data points also increases significantly when the two modifications are included in the processing. Unrealistic negative densities are excluded from the correlation analysis, and the increased number of data points indicates that the occurrence of such unrealistic densities is greatly reduced. Therefore the actual improvement is even larger. Also for Swarm-B, including the direct estimation of aerodynamic acceleration results in the largest improvement, but slight improvements in correlation and standard deviation are visible when the new satellite geometry and aerodynamic

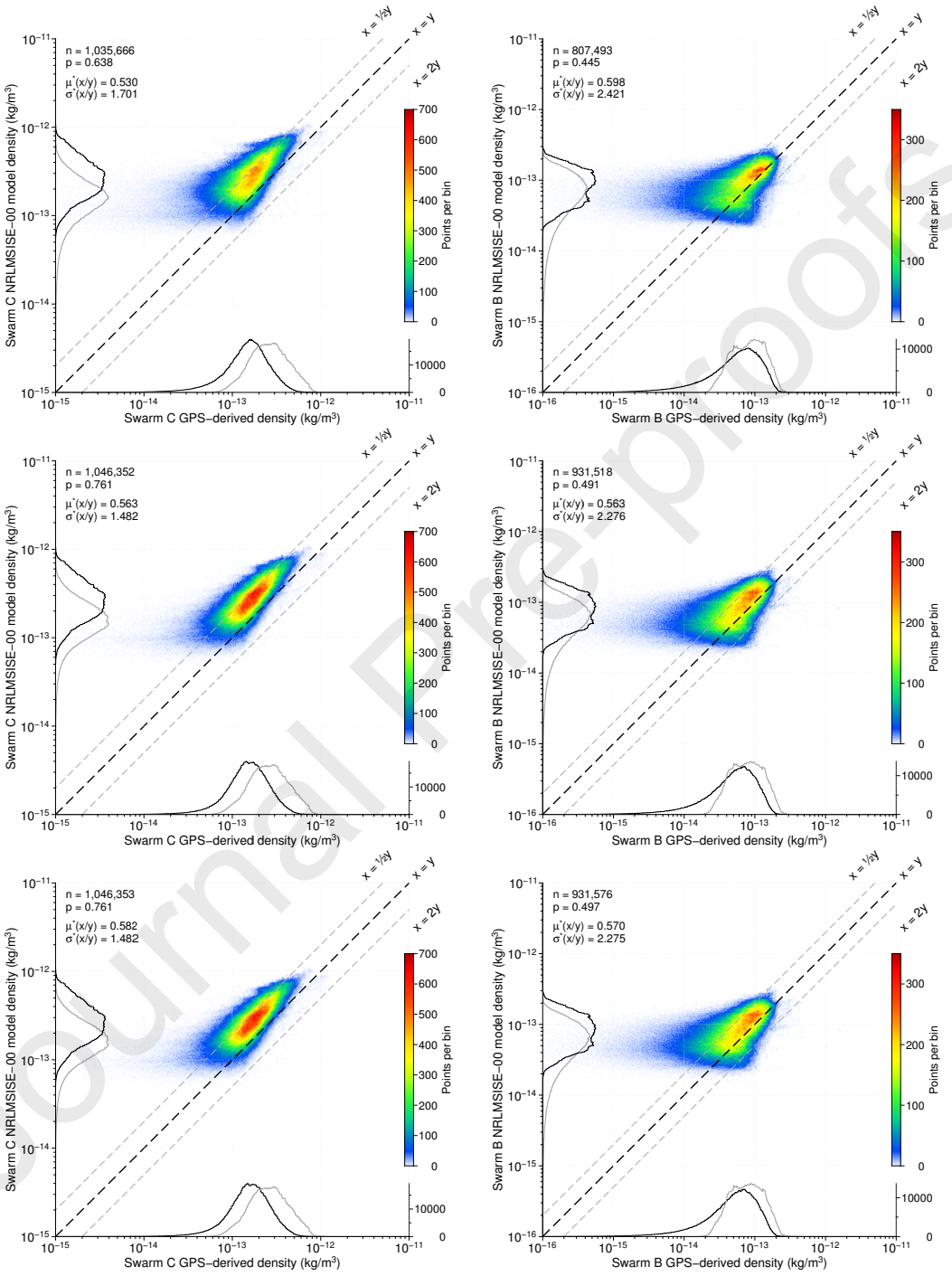


Figure 8: Estimated versus modelled densities for Swarm-C (left) and Swarm-B (right) for 2018 with the original strategy (top), the direct estimation of aerodynamic accelerations (middle) and the additional new aerodynamic and geometry modelling (bottom).

model is used. With the latest processing strategy, the mean of the density ratios for the two satellites is more comparable, which indicates that satellite dependent processing errors are reduced for the estimated densities.

The accuracy of the GPS-derived thermospheric densities is limited by the uncertainties in the estimation of the aerodynamic accelerations, the direct algorithm used to derive the densities, the modelling of the horizontal winds and radiation pressure accelerations, as well as the determination of the force coefficient. Doornbos et al. (2010) show that the use of the direct algorithm leads to density retrieval errors of about 0.7% of the total density signal, while neglecting winds results in an error of about 2.2%. They also show that a 5% variation in the accommodation coefficient leads to a relative density error of about 1.9%. Their analysis was based on one year of CHAMP data from 2004, but it is expected that these errors have a similar order of magnitude for the Swarm satellites, because of their similar altitude and elongated satellite design.

For the Swarm satellites, it is clear from the results shown in figure 8, that for low thermospheric densities, radiation pressure modelling errors are a significant error source. In section 2.1 it is assessed that the modelling of the radiation pressure accelerations has an uncertainty of about 6.4%, as indicated by the standard deviation of the estimated daily solar radiation pressure scale factor for the higher-flying Swarm-B satellite. According to figure 2, the radiation pressure accelerations experienced by the Swarm satellites can be up to 40 $nm/s^2$, which leads to an uncertainty of about 2.6 $nm/s^2$. Based on equation 1, this uncertainty in acceleration can be roughly converted into an error in the derived density. Assuming a satellite velocity of 7.5 km/s, a reference area of 1 $m^2$, a satellite mass of approximately 400 kg and a force coefficient value of about 3.2 (see March et al. (2019a)), this results in a density error due to radiation pressure modelling errors of about 1.1 $10^{-14}$ $kg/m^3$. Note that the relatively large force coefficient value obtained for Swarm is due to the large contribution of random thermal motion collisions of lightweight constituents along the elongated satellite shape, which is usually ignored for compact satellite shapes (Doornbos et al., 2010).

The uncertainty in the estimation of the aerodynamic accelerations can be assessed using overlap analysis of the estimated empirical accelerations. However, certain types of systematic errors may not be revealed using overlap analysis, therefore overlap errors might underestimate the true errors. As indicated in section 2, the GPS data are processed in 30 h arcs, with a 6 h overlap between consecutive solutions. To avoid possibly larger errors

at the edges of the orbit solution, the first and last hour of each overlap are ignored in the overlap analysis. Using one year of data from 2018, the RMS error of the overlapping aerodynamic accelerations obtained with the latest processing strategy is about 0.7 nm/s$^2$ for Swarm-B, while for Swarm-C the RMS error is about 0.8 nm/s$^2$. Using again equation 1, this roughly translates to density errors of about 0.3 $10^{-14}$ kg/m$^3$ and 0.4 $10^{-14}$ kg/m$^3$ for, respectively, Swarm-B and Swarm-C.

It is shown that especially for the higher-flying Swarm-B satellite, it is difficult to obtain accurate densities during low solar activity conditions. Assuming that under those conditions the density variability with respect to the orbit mean indicates an error instead of signal, it is possible to obtain an indication of the estimated density error. Using GPS-derived Swarm-B densities for the period April-July 2019, which is a period with very low solar activity, this results in a density error of about 3.3 $10^{-14}$ kg/m$^3$. During this time frame, the Swarm-B densities have an RMS signal of about 5.6 $10^{-14}$ kg/m$^3$, which means that the relative density error is almost 60%. For the same period in 2014 during high solar activity, the estimated densities have an RMS signal of about 4.5 $10^{-13}$ kg/m$^3$, which results in a relative density error of about 7%. Assuming a similar density error for the lower pair results in relative errors of 4% and 19%, during high and low solar activity, respectively.

It is expected that part of the Swarm-B density variability in April-July 2019 represents signal instead of error and therefore this density error should be regarded as a conservative error estimate. On the other hand, it is assumed that the absolute density estimation error is independent of the aerodynamic signal size. While this is true for the radiation pressure induced error, the density error due to uncertainties in the aerodynamic modelling is dependent on the aerodynamic signal size, and therefore the resulting density error due to this uncertainty might be slightly higher for the lower pair and during high solar activity.

## 4. Conclusions

Because of the many anomalies in the Swarm accelerometer data, an alternative approach has been developed, where the high-quality GPS data are used to derive the non-gravitational accelerations acting on the Swarm satellites. In order to convert the range and phase information in the Swarm GPS measurements into accelerations, a precise orbit determination approach is

used, in which gravitational accelerations are modelled with a very high fidelity, and the non-gravitational accelerations are part of the parameters to be estimated. In addition, a second processing chain has been developed which also includes modelled radiation pressure accelerations, in order to derive aerodynamic-only accelerations from the GPS data.

The estimated non-gravitational accelerations are used to correct and augment the accelerometer observations for Swarm-C, which are used to generate high-resolution thermosperic densities for this satellite. The GPS-only aerodynamic accelerations are used to derive thermospheric densities with a lower temporal resolution of about 20 minutes. These densities are available for all Swarm satellites. The Swarm GPS-only densities are expected to be very useful for the calibration of thermospheric density models. The DTM2018 density model, which is an intermediate update of the DTM2013 model (Bruinsma, 2015), notably includes three years of GPS-derived Swarm-A density data in addition to the accelerometer-derived density data from the CHAMP, GRACE and GOCE satellites. For the analysis of high-frequency phenomena, however, the relatively smooth GPS-only densities are not suited and only the merged GPS-accelerometer densities can be used.

Weimer et al. (2018) used the GPS-derived densities to study the thermosphere's semi-annual variation, for which the low temporal resolution limitations of the data were not an issue. Astafyeva et al. (2017) show that GPS-derived Swarm densities can be used to study effects of storms in the thermosphere on a global level and to identify differences in the response between the local time sectors, latitude sectors and altitudes samples by the three Swarm satellites. However, they also indicate that, due to their relatively low temporal resolution compared to accelerometers, these densities cannot be used to identify localized density variations and identify traveling disturbances. All Swarm thermospheric densities, as well as the estimated non-gravitational accelerations and aerodynamic accelerations are available for users at the dedicated ESA Swarm website (ftp://swarm-diss.eo-int).

Two modifications have recently been applied to the Swarm density retrieval processing strategy. They consist of a more refined handling of solar and Earth radiation pressure accelerations in the additional processing chain for the estimation of aerodynamic accelerations, and the use of a more realistic high-fidelity satellite geometry and aerodynamic model for the conversion of aerodynamic accelerations to thermospheric densities. It is shown that the correlation between estimated densities and NRLMSISE-00 model densities significantly improves when these modifications are included in the density

processing. Based on one year of data in 2018, which had low solar activity, for Swarm-C the correlation improves from 0.64 to 0.76, and the standard deviation of the density ratios reduces from 1.70 to 1.48. For Swarm-B, the correlation also improves from 0.45 to 0.50. However, for this higher-flying satellite, the smaller density signal leads to relatively higher processing errors. With the current low solar activity, the Swarm satellites experience very low atmospheric drag and therefore it is becoming more difficult to resolve latitudinal density variability using GPS data, especially for the higher-flying satellite. In these circumstances, mean orbit density values are more reliable and these values are also included in the available Level 2 Swarm thermospheric density product.

For future work, it is planned to further improve the radiation pressure modelling of the Swarm satellites by also using a more realistic satellite surface geometry model for the modelling of this force. With this model, the tuning of the optical properties of the different satellite surfaces will also be analysed. In addition, the selection of the optimal accommodation coefficient for the gas-surface interaction will be further investigated. These investigations might further improve the Swarm densities, especially for low solar activity conditions.

## Acknowledgements

The authors gratefully acknowledge ESA for the provision of the Swarm data. Parts of the work described in this study were financed through ESA contract no. 4000102140/10/NL/JA.

## References

Astafyeva, E., Zakharenkova, I., Huba, J., Doornbos, E., Van den IJssel, J. 2017, Global ionospheric and thermospheric effects of the June 2015 geomagnetic disturbances: multi-instrumental observations and modeling, Journal of Geophysical Research: Space Physics 122(11), 11716-11742, doi:10.1002/2017JA024174.

Bezděk, A., Sebera, J., Klokočník, J. 2018, Calibration of Swarm accelerometer data by GPS positioning and linear temperature correction, Advances in Space Research 62(2), 317-325, doi:10.1016/j.asr.2018.04.041.

Bowman, B.R., Marcos, F.A., Moe, K., Moe, M. 2007, Determination of drag coefficient values for CHAMP and GRACE satellites using orbit drag analysis, Astrodynamics Specialist Conference, American Astronomical Society, Mackinac Island, MI, AAS 07-259.

Bruinsma, S., Tamagnan, D., Biancale, R. 2004, Atmospheric densities derived from CHAMP/STAR accelerometer observations, Planetary and Space Science 52(4), 297-312.

Bruinsma, S. (2015) The DTM-2013 thermosphere model, Journal of Space Weather and Space Climate, 5(A1), 1-8, doi:10.1051/swsc/2015001.

Calabia, A., Jin, S. 2017, Thermospheric density estimation and response to the March 2013 geomagnetic storm from GRACE GPS-determined precise orbits, Journal of Atmospheric and Solar-Terrestrial Physics 154, 167-179, doi:10.1026/j.jastp.2016.12.011.

Cerri, L., Berthias, J., Bertiger, W., Haines, B., Lemoine, F., Mercier, R., Ries, J., Willis, P., Zelensky, N., Ziebart, M. 2010, Precision orbit determination standards for the Jason series of altimeter missions, Marine Geodesy 33(S1), 379-418, doi:10.1080/01490419.2010.488966.

Dach, R., Brockmann, E., Schaer, S., Beutler, G., Meindl, M., Prange, L., Bock, H., Jäggi, A., Ostini, L. 2009, GNSS processing at CODE: status report, Journal of Geodesy 83(3-4), 353-365.

Dach, R., Schaer, S., Arnold, D., Prange, L., Sidorov, D., Stebler, P., Villiger, A., Jäggi, A. 2018, CODE final product series for the IGS, Astronomical Institute, University of Bern, doi:10.7892/boris.75876.3.

Doornbos, E., Van den IJssel J., Lühr, H., Förster, M., Koppenwallner, G. 2010, Neutral density and crosswind determination from arbitrarily oriented multiaxis accelerometers on satellites, Journal of Spacecraft and Rockets 47(4), 580-589.

Doornbos, E. 2012, Thermospheric density and wind determination from satellite dynamics, Springer Theses, Springer-Verlag Berlin Heidelberg, doi:10.1007/978-3-642-25129-0.

Drob, D., Emmert, J., Crowley, G., Picone, J., Shepherd, G., Skinner, W., Hays, P., Niciejewski, R., Larsen, M., She, C., Meriwether, J., Hernandez, G., Jarvis, M., Sipler, D., Tepley, C., O'Brien, M., Bowman, J., Wu, Q., Murayama, Y., Kawamura, S., Reid, I., Vincent, R. 2008, An empirical model of the Earth's Horizontal Wind Fields: HWM07, Journal of Geophysical Research 113(A12304), 1-18, doi:10.1029/2008JA013668.

Fedosov, V., Peřestý, R. 2011, Measurement of microaccelerations on board of the LEO spacecraft, Proceedings of the 18th IFAC World Congress, Vol. 18, 1883-1388.

Friis-Christensen, E., Lühr, H., Knudsen, D., Haagmans, R. 2008, Swarm - an earth observation mission investigating geospace, Advances in Space Research, 41(1), 210-216, doi:10.1016/j.asr/2006.10.008.

Gallis, M., Torczynski, J., Plimpton, S., Rader, D., Koehler, T. 2014, Direct simulation Monte Carlo: the quest for speed. In: AIP Conference Proceedings 1628, 27-36. doi:10.1063/1.4902571.

Knocke, P., Ries, J., Tapley B. 1988, Earth radiation pressure effects on satellites. In: AIAA/AAS astrodynamics conference, 577-587.

Kuang, D., Desai, S., Sibthorpe, A., Pi, X. 2014, Measuring atmospheric density using GPS-LEO tracking data, Advances in Space Research 53(2), 243-256, doi:10.1016/j.asr.2013.11.022.

Lyard, F., Lefevre, F., Letellier, T., Francis, O. 2006, Modelling the global ocean tides: modern insights from FES2004, Ocean Dynamics 56(5-6), 394-415, doi:10.1007/s10236-006-0086-x.

March, G., Doornbos, E., Visser, P. 2019a, High-fidelity geometry models for improving the consistency of CHAMP, GRACE, GOCE and Swarm thermospheric density data sets, Advances in Space Research 63(1), 213-238, doi:10.1016/j.asr.2018.07.009.

March, G., Visser, T., Visser, P., Doornbos, E. 2019b, CHAMP and GOCE thermospheric wind characterization with improved gas-surface interactions modelling, Advances in Space Research 64(6), 1225-1242, doi:10.1016/j.asr.2019.06.023.

Marcos, F., Bass, J., Baker, C., Borer, W. 1994, Neutral density models for aerospace applications. In: 32nd Aerospace sciences meeting & exhibit, Reno, NV., AIAA 94-0589, doi: 10.2514/6.1994-589.

Mayer-Gürr, T., Rieser, D., Höck, E., Brockmann, J., Schuh, W., Krasbutter, I., Kusche, J., Maier, A., Kraus, S., Hausleitner, W., Bauer, O., Jäggi, A., Meyer, U., Prange, L., Pail, R., Fecher, T., Gruber, T. 2012, The new combined satellite only model GOCO03s, Paper S2183. GGHS Meeting in Venice, Italy, 912 October 2012.

McCarthy, D., Petit, G. 2004, IERS conventions 2003, IERS technical note no. 32, Bundesamt für Kartographie und Geodeäsie, Frankfurt am Main, Germany.

McLaughlin, C. Lechtenberg, T., Fattig, E., Mysore Krishna, D. 2013, Estimating density using precision satellite orbits from multiple satellites, Journal of Astronautical Science 59(1-2), 84-100, doi:10.1007/s40295-013-0007-4.

Mehta, P., Walker, A., Sutton, E., Godinez, H. 2017, New density estimates derived using accelerometers on board the CHAMP and GRACE satellites Space Weather 15(4), 558-576, doi:10.1002/2016SW001562.

Montenbruck, O., Van Helleputte, T., Kroes, R., Gill, E. 2005, Reduced dynamic orbit determination using GPS code and carrier measurements, Aerospace Science and Technology 9, 261-271, doi:10.1016/j.ast.2005.01.003.

Montenbruck, O., Hackel, S., Van den IJssel, J, Arnold, D. 2018, Reduced dynamic and kinematic precise orbit determination for the Swarm mission from 4 years of GPS tracking, GPS Solutions 22(79), 1-11, doi:10.1007/s10291-018-0746-6.

Pardini, C., Anselmo, L., Moe, K., Moe, M. 2010, Drag and energy accommodation coefficients during sunspot maximum, Advances in Space Research 45(5), 638-650, doi:10.1016/j.asr.2009.08.034.

Picone, J., Hedin, A., Drob, D., Aikin, A. 2002, NRLMSISE-00 empirical model of the atmosphere: statistical comparisons and scientific issues, Journal of Geophysical Research 107(A12), 1-16, doi:10.1029/2002JA009430.

Pilinski, M.D., Argrow, B.M., Palo, S.E. 2010, Semiempirical model for satellite energy-accommodation coefficients, Journal of Spacecraft and Rockets 47(6), 951-956, doi:10.2514/1.49330.

Schmid, R., Dach, R., Collilieux, X., Jäggi, A., Schmitz, M., Dilssner, F. 2016, Absolute IGS antenna phase center model igs08.atx: status and potential improvements, Journal of Geodesy 90, 343-364, doi:10.1007/s00190-015-0876-3.

Sentman, L. 1961a, Comparison of the exact and approxiamte methods for predicting free molecule aerodynamic coefficients, American Rocket Society Journal 31(11), 1576-1579.

Sentman, L. 1961b, Free molecule flow theory and its application to the determination of aerodynamic forces, TR LMSC-448514, Lockheed Missile and Space Co., Sunnyvale CA.

Siemes, C., Teixeira da Encarnação, J., Doornbos, E., Van den IJssel, J., Kraus, J., Pereštý, R., Grunwaldt, L., Apelbaum, G., Flury, J., Olsen, P.E. 2016, Swarm accelerometer data processing from raw accelerometers to thermospheric densities, Earth, Planets and Space 68(92), 1-16, doi:10.1186/s40623-016-0474-5.

Siemes, C. 2019, Swarm satellite thermo-optical properties and external geometry, ESA-EOPG-MOM-MO-15, 1-12.

Sutton, E., Nerem, R., Forbes, J. 2007, Density and winds in the thermosphere deduced from accelerometer data, Journal of Spacecraft and Rockets 44(6), 1210-1219, doi:10.2514/1.28641.

Sutton, E.K. 2008, Effects of solar disturbances on the thermospheric densities and winds from CHAMP and GRACE satellite accelerometer data, Ph.D. thesis, University of Colorado at Boulder.

Teixeira da Encarnação, J., Arnold, D., Bezděk, A., Dahle, C., Doornbos, E., Van den IJssel, J., Jäggi, A., Mayer-Gürr, T., Sebera, J., Visser, P., Zehentner, N. 2016, Gravity field models derived from Swarm GPS data, Earth, Planets and Space 68(127), 1-15, doi:10.1186/s40623-016-0499-9.

Van den IJssel, J., Teixeira da Encarnação, J., Doornbos, E., Visser, P. 2015, Precise science orbits for the Swarm satellite constellation, Advances in Space Research 56(6), 1042-1055, doi:10.1016/j.asr.2015.06.002.

Van den IJssel, J., Forte, B., Montenbruck, O. 2016, Impact of Swarm GPS receiver updates on POD performance, Earth, Planets and Space 68(85), 1-17, doi:10.1186/s40623-016-0459-4.

Vielberg, K., Forootan, E., Lück, C., Löcher, A., Kusche, J., Börger, K. 2018, Comparison of accelerometer data calibration methods used in thermospheric neutral density estimation, Annales Geophysicae 36(3), 761-779, doi:10.5194/angeo-36-761-2018.

Visser, P., Doornbos, E., Van den IJssel, J., Teixeira da Encarnação, J. 2013, Thermospheric density and wind retrieval from Swarm observations, Earth, Planets and Space, 65(11), 1319-1331, doi:10.5047/eps.2013.08.003.

Visser, T., March, G., Doornbos, E., De Visser, C., Visser, P. 2019, Horizontal and Vertical Thermospheric Cross-Wind from GOCE Linear and Angular Accelerations, Advances in Space Research 63(10), 3139-3153, doi:10.1016/j.asr.2019.01.030.

Visser, P., Van den IJssel, J. 2016, Orbit determination and estimation of non-gravitational accelerations for the GOCE reentry phase, Advances in Space Research 58(9), 1840-1853, doi:10.1026/j.asr.2016.07.013.

Weimer, D.R., Mlynczak, M.G., Emmert, J., Doornbos, E., Sutton, E.K., Hunt, L.A. (2018), Correlations between the Thermosphere's Semiannual Density Variations and Infrared Emissions Measured with the SABER Instrument, Journal of Geophysical Research: Space Physics 123(10), 8850-8864, doi:10.1029/2018JA025668.

Wermuth, M., Montenbruck, O., Van Helleputte, T. 2010, GPS high precision orbit determination software tools (GHOST), Proceedings of the 4th International Conference on Astrodynamics Tools and Techniques, Madrid, 3-6.

Zangerl, F., Griesauer, F., Sust, M., Montenbruck, O., Buchert, B., Garcia, A. 2014, Swarm GPS precise orbit determination receiver intitial inorbit performance evaluation, Proceedings of the 27th International Tech-

nical Meeting of the Satellite Division of the Institute of Navigation (ION GNSS+), Tampa, Florida, 1459-1468.

GPS-derived thermosphere densities are available for all Swarm satellites

These densities have a temporal resolution of about 20 minutes

Two recent processing modifications improve the density retrieval accuracy

**Declaration of interests**

☒ The authors declare that they have no known competing financial interests or personal relationships that could have appeared to influence the work reported in this paper.

☐The authors declare the following financial interests/personal relationships which may be considered as potential competing interests: